CIRCUITS SYSTEMS SIGNAL PROCESSING
VOL. 22, NO. 2, 2003, PP. 193–210

OPTIMIZED PROTOTYPE FILTER BASED ON THE FRM APPROACH FOR COSINE-MODULATED FILTER BANKS*

Miguel B. Furtado Jr.,[1] *Paulo S. R. Diniz,*[1] *and Sergio L. Netto*[1]

Abstract. A design procedure for frequency-response masking (FRM) prototype filters of cosine-modulated filter banks (CMFBs) is proposed. In the given method, we perform minimization of the maximum attenuation level in the filter's stopband, subject to intersymbol interference (ISI) and intercarrier interference (ICI) constraints. For optimization, a quasi-Newton algorithm with line search is used, and we provide simplified analytical expressions to impose the interference constraints, which greatly reduce the computational complexity of the optimization procedure. The result is lower levels of ISI and ICI for a predetermined filter order, or a reduced filter complexity for given levels of interferences. It is then illustrated how the FRM-CMFB structure is suitable for implementing filter banks with a large number of bands, yielding sharp transition bands and small roll-off factors, which is an attractive feature for a wide range of practical applications.
Key words: filter banks, cosine-modulated filter banks, frequency-response masking, high resolution spectrum analysis.

1. Introduction

Cosine-modulated filter banks (CMFBs) are commonly used in practice because of two main features [1], [9], [11]. First, their realization relies only on the design of a single prototype filter that reduces the total number of parameters to be specified. Second, CMFBs have computationally efficient implementations based on fast algorithms for the discrete cosine transform (DCT). For very demanding applications where maximum selectivity is required, the prototype filter for the CMFB tends to present a very high order, thus increasing the computational complexity of the overall structure. A possible design procedure that avoids this problem is to use the frequency-response masking (FRM) approach [6] for

* Received January 11, 2002; revised October 18, 2002.
[1] Programa de Engenharia Elétrica, COPPE/EPoli/UFRJ, P. O. Box 68504, Rio de Janeiro, RJ, 21945-970, Brazil. E-mail for Furtado: furtado@lps.ufrj.br E-mail for Diniz: diniz@lps.ufrj.br E-mail for Netto: sergioln@lps.ufrj.br

designing the CMFB prototype filter. This technique is known to produce sharp linear-phase FIR filters with a reduced number of coefficients, resulting in the *FRM-CMFB structure* [3].

This paper presents an optimization procedure of the FRM-CMFB prototype filter aiming at the reduction of the maximum stopband magnitude, with constraints on the intersymbol interference (ISI) and intercarrier interference (ICI) of the overall structure. It is then verified that the reduced number of coefficients required by the FRM approach not only may generate a more efficient structure in terms of computational complexity but also leads to a simpler and faster optimization problem. The optimization procedure is based on variations of sequential quadratic programming, using a constrained quasi-Newton method with line search. A simplified analytical derivation of the interference constraints is given, which greatly speeds up the optimization procedure. The results include lower levels of ISI and ICI for a fixed filter order, or a reduced filter bank complexity for given levels of interferences.

The remainder of the paper is organized as follows: In Section 2, descriptions of the CMFB structure and the transmultiplexer (TMUX) configuration are given. In Section 3, a brief explanation of the FRM approach for designing low-complexity FIR filters is provided. In Section 4, the FRM-CMFB implementation is then presented as an efficient alternative to design highly selective filter banks. In Section 5, the optimization procedure for the FRM-CMFB prototype filter is presented with emphasis given on a simplified analytical derivation for the interference constraints. Finally, Section 6 includes some design examples, showing improved results achieved with the optimized FRM-CMFB structure.

2. The CMFB and TMUX systems

CMFBs are easy-to-implement structures based on a single prototype filter, whose modulated versions will form the analysis and synthesis subfilters of the complete bank [10]. The modulation operation is implemented in an efficient manner by using fast algorithms for the DCT. Usually, the prototype filter for an M-band filter bank is specified by its 3 dB attenuation point and the stopband edge at frequencies

$$\omega_{3dB} \approx \frac{\pi}{2M} \quad \text{and} \quad \omega_s = \frac{(1+\rho)\pi}{2M}, \tag{1}$$

respectively, where ρ is called the *roll-off factor*.

Assuming that the prototype filter has an impulse response $h_p(n)$ of order N_p, its transfer function is expressed as

$$H_p(z) = \sum_{n=0}^{N_p} h_p(n) z^{-n}. \tag{2}$$

Thus impulse response of the analysis and synthesis subfilters are then

cosine-modulated versions of the prototype filter, which can be described by

$$h_m(n) = h_p(n)c_{m,n} \tag{3}$$

$$f_m(n) = h_p(n)\bar{c}_{m,n} \tag{4}$$

for $m = 0, 1, \ldots, (M-1)$ and $n = 0, 1, \ldots, N_p$, where

$$c_{m,n} = 2\cos\left[\frac{(2m+1)(n-N_p/2)\pi}{2M} + (-1)^m\frac{\pi}{4}\right] \tag{5}$$

$$\bar{c}_{m,n} = 2\cos\left[\frac{(2m+1)(n-N_p/2)\pi}{2M} - (-1)^m\frac{\pi}{4}\right]. \tag{6}$$

If the prototype filter has $(N_p+1) = 2KM$ coefficients, then it can be decomposed into $2M$ polyphase components

$$H_p(z) = \sum_{j=0}^{2M-1} z^{-j}E_j(z^{2M}) \tag{7}$$

with $E_j(z)$ for $j = 0, 1, \ldots, (2M-1)$ given by

$$E_j(z) = \sum_{k=0}^{K-1} h_p(2kM+j)z^{-k}. \tag{8}$$

Therefore, using the fact that $c_{m,(n+2kM)} = (-1)^k c_{m,n}$, the analysis filter can be written as

$$\begin{aligned} H_m(z) &= \sum_{j=0}^{2M-1}\sum_{k=0}^{K-1} c_{m,(2kM+j)}h_p(2kM+j)z^{-(2kM+j)} \\ &= \sum_{j=0}^{2M-1}\left[c_{m,j}z^{-j}\sum_{k=0}^{K-1}(-1)^k h_p(2kM+j)z^{-2kM}\right] \\ &= \sum_{j=0}^{2M-1} c_{m,j}z^{-j}E_j(-z^{2M}). \end{aligned} \tag{9}$$

With this polyphase decomposition, it can be shown that all filtering operations can be performed using sparse matrix multiplications involving an identity matrix, a reversed identity matrix, and a DCT-IV operation, leading to a reduced number of operations per output sample [10]. Notice that although we concentrate our presentation here on the analysis filters, an entirely similar reasoning applies to the synthesis filters, and is omitted due to the paper length limitations. Figure 1 shows the block diagram of the filter bank described above, with the input-output relation described by

$$\hat{Y}(z) = \frac{1}{M}\left[T_0(z)Y(z) + \sum_{i=1}^{M-1} T_i(z)Y(ze^{\frac{j2\pi i}{M}})\right]. \tag{10}$$

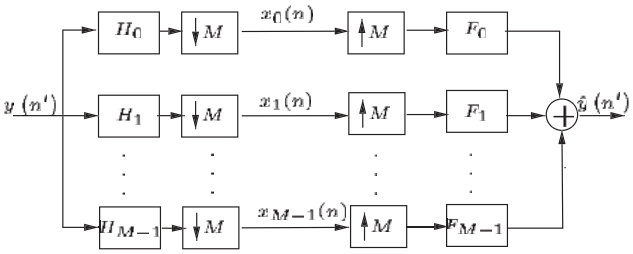

Figure 1. M-channel maximally decimated filter bank.

The first term in equation (10), $T_0(z)$, is the direct transfer function and must be the only term in an alias-free design, which includes the perfect reconstruction (PR) filter bank, as a particular case. The second term, involving all other $T_i(z)$, contains the aliasing transfer functions, which quantify the influences in a given band from all other bands. These terms are expressed by

$$T_0(z) = \sum_{m=0}^{M-1} F_m(z) H_m(z) \tag{11}$$

$$T_i(z) = \sum_{m=0}^{M-1} F_m(z) H_m(z e^{\frac{-j2\pi i}{M}}). \tag{12}$$

The maximally decimated M-channel TMUX system is a filter bank where the analysis and synthesis blocks are switched, in order to form a system with M input/output channels, as depicted in Figure 2 [5], [10]. This structure interpolates and filters each input signal, adding the resulting signals on each branch to form a single signal for transmission over a given channel C. At the receiver, the signal is then split back into M channels to generate the desired M outputs. The design problem of such a system can be simplified by assuming that the channel response is ideal ($C \equiv 1$), or a pure delay. Then, in the PR case, each output signal is identical to its equivalent input, whereas in the nearly PR (NPR) case, a small interference among the subchannels is present.

The general relation that describes the transfer functions of the TMUX system is given by

$$\hat{\mathbf{x}}(z^M) = \frac{1}{M} \mathbf{T}(z^M) \mathbf{x}(z^M), \tag{13}$$

where

$$\hat{\mathbf{x}}(z) = [\hat{X}_0(z)\ \hat{X}_1(z)\ \ldots\ \hat{X}_{M-1}(z)]^T \tag{14}$$

$$\mathbf{x}(z) = [X_0(z)\ X_1(z)\ \ldots\ X_{M-1}(z)]^T \tag{15}$$

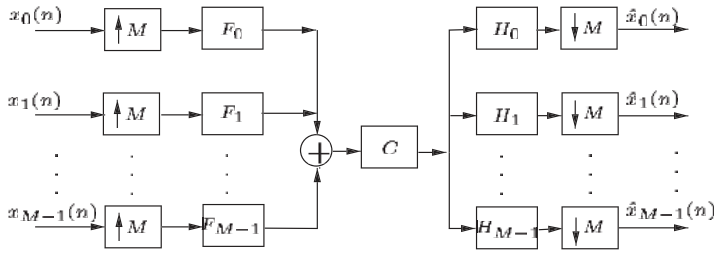

Figure 2. M-channel maximally decimated TMUX system.

and

$$[\mathbf{T}(z^M)]_{ab} = \sum_{m=0}^{M-1} H_a(ze^{-\frac{j2\pi m}{M}})F_b(ze^{-\frac{j2\pi m}{M}}) \tag{16}$$

for $a, b = 0, 1, \ldots, (M-1)$. The matrix $\mathbf{T}(z^M)$ is the transfer matrix whose elements, $[\mathbf{T}(z^M)]_{ab}$, represent the transfer function between the interpolated input a and the decimated output b. Thus, the main diagonal entries of this matrix, $[\mathbf{T}(z^M)]_{aa}$, represent the transfer functions of each channel, and the other terms give the crosstalk between two different channels. In the NPR case, no restrictions apply to the transfer matrix, whereas in the PR case, the crosstalk terms must be zero and the diagonal terms become simple delays [12].

In a TMUX system, one would be interested in estimating the total ISI and ICI figures of merit, which are given by [12]:

$$\text{ISI} = \max_a \left\{ \sum_n [\delta(n) - t_a(n)]^2 \right\} \tag{17}$$

$$\text{ICI} = \max_{a,\omega} \left\{ \sum_{b=0, a\neq b}^{M-1} |[\mathbf{T}(e^{j\omega})]_{ab}|^2 \right\}, \tag{18}$$

where $\delta(n)$ is the ideal impulse, $t_a(n)$ is the impulse response for the ath channel, and the term $[\mathbf{T}(e^{j\omega})]_{ab}$ is the crosstalk between the ath and bth channels, whose expression is given by equation (16).

3. The FRM approach

The FRM technique [6] is an efficient method to design FIR filters with arbitrary passband and sharp transition bands with reduced number of coefficients. The basic principle behind the FRM approach consists of the use of a complementary pair of interpolated linear-phase FIR filters. The base filter, $H_b(z)$, and its complementary version, $H_{b_c}(z)$ are interpolated by a factor of L to form sharp transition bands, at the cost of introducing multiple passbands on each frequency

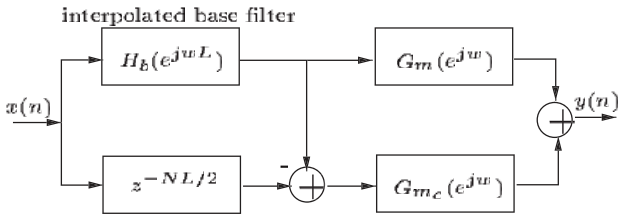

Figure 3. FRM structure: The interpolated complementary pair of filters and the respective masking filters work together to produce the desired frequency response.

response. These repetitive passbands are then filtered out by the positive and negative masking filters, denoted by $G_m(z)$ and $G_{m_c}(z)$, respectively, and added together to compose the overall desired filter, $H_f(z)$. This overall procedure is illustrated in Figure 3 and described by

$$H_f(z) = H_b(z^L)G_m(z) + H_{b_c}(z^L)G_{m_c}(z). \tag{19}$$

If the base filter is a linear-phase FIR filter of even order N_b, such that its L-interpolated transfer function is given by

$$H_b(z^L) = \sum_{i=0}^{N_b} h_b(i)z^{-Li}, \tag{20}$$

then its complementary filter can be obtained as

$$H_{b_c}(z^L) = z^{-N_bL/2} - \sum_{i=0}^{N_b} h_b(i)z^{-Li} \tag{21}$$

in such a manner that

$$|H_b(e^{j\omega L}) + H_{b_c}(e^{j\omega L})| = 1 \tag{22}$$

as is desired.

The design of the base filter is strictly dependent on the desired bandedge frequencies ω_p and ω_s and on the interpolation factor L. These parameters determine the cutoff frequencies θ and ϕ, which determine the transition edges of the prototype filter. Figures 4a and 4b show the base filter and the complementary filter characteristics. The design of the masking filters also depends on the interpolation factor L and on the cutoff frequencies θ and ϕ, used to build the complementary pair. In practice, L may be chosen such that the total number of coefficients of the overall FRM filter is minimized, as given in [7]. The subfilters can still be optimized depending on the application, as described in [2], [4].

An important feature can be observed if the desired frequency response requires both the passband and transition band to be narrow. This case may lead to implementations that do not require the negative lower branch of the FRM structure, further reducing the number of coefficients required in the overall filter.

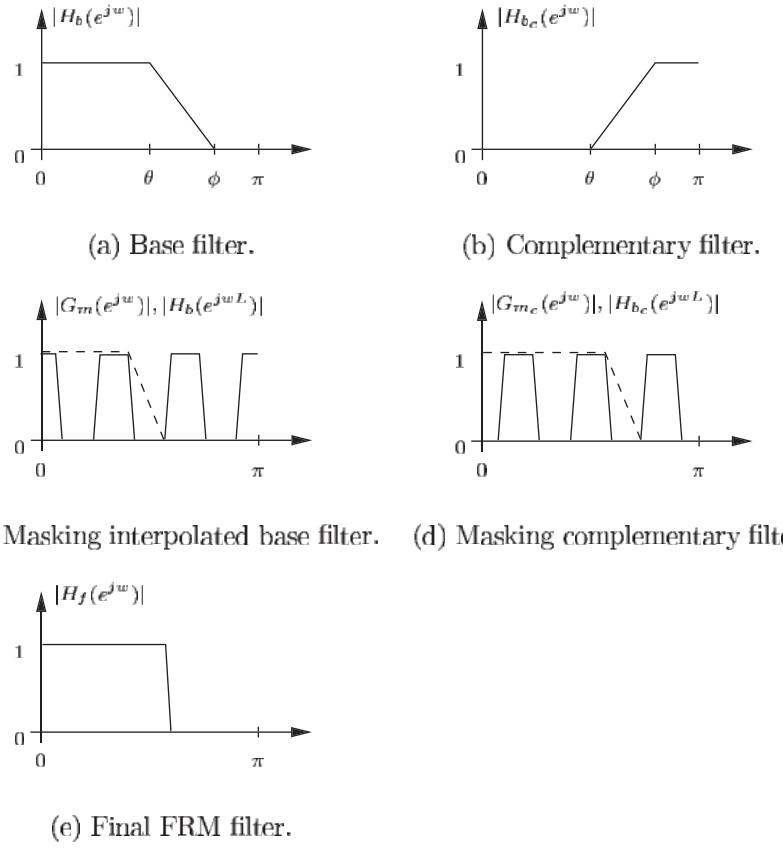

Figure 4. The FRM approach: Combining the positive and negative branches of the structure to form the overall frequency response, with arbitrary passband and narrow transition band.

Applications where prototype filters are developed for maximally decimated filter banks with a large number of bands fall into this category.

4. The FRM-CMFB structure

From the analysis of the FRM and the CMFB schemes, an efficient FRM-CMFB joint structure can be derived if the interpolation factor L for the FRM filter can be written as [3]

$$L = 2K_aM + \frac{M}{K_b} \tag{23}$$

where $K_a \geq 0$ and $K_b > 0$ are integer numbers. In such a case, using solely the upper branch on the FRM scheme, the mth analysis filter can be written as

$$H_m(z) = \sum_{i=0}^{N_b} \left[h_b(i) z^{-Li} \sum_{n=0}^{N_m} c_{m,[n+Li]} g_1(n) z^{-n} \right], \tag{24}$$

where N_m is the order and $g_1(n)$ are the coefficients of the masking filter. Notice that for the general FRM structure, a similar description should be obtained for the lower branch, and the results for both branches added together. Hence, from equation (24), by using $Q = 2K_b$ polyphase components for the base filter, with $i = kQ + q$ and $(N_b + 1) = QK_c$, we obtain, after some manipulations,

$$H_m(z) = \sum_{q=0}^{Q-1} \sum_{k=0}^{K_c-1} \left[h_b(kQ+q) z^{-L(kQ+q)} (-1)^{(k+K_a q)} \sum_{n=0}^{N_m} c_{m,(n+\frac{M}{K_b}q)} g_1(n) z^{-j} \right]. \tag{25}$$

By writing the modified polyphase components of the interpolated base filter as

$$H'_{b1q}(z) = \sum_{k=0}^{K_c-1} (-1)^{K_a q} h_b(kQ + q) z^{-k} \tag{26}$$

for $q = 0, 1, \ldots, (Q - 1)$, and by using the masking filter polyphase component given by

$$E'_j(z) = \sum_{k=0}^{K_d-1} g_1(2kM + j) z^{-k} \tag{27}$$

for $j = 0, 1, \ldots, (2M - 1)$, equation (25) becomes

$$H_m(z) = \sum_{q=0}^{Q-1} \left[z^{-Lq} H'_{b1q}(-z^{LQ}) \sum_{j=0}^{2M-1} c_{m,(n+\frac{M}{K_b}q)} z^{-j} E'_j(-z^{2M}) \right]. \tag{28}$$

This relation leads to the structure depicted in Figure 5, where the value of K is equivalent to the CMFB case (see equation (8)).

The values of K_a and K_b can be chosen such that the overall filter has the same order as required by the standard CMFB design. In such cases, it is easier to compare the structures of the FRM-CMFB and the standard CMFB.

5. Optimized FRM-CMFB

Standard optimization goals for the CMFB prototype filter are to minimize the objective functions

$$E_2 = \int_{\omega_s}^{\pi} |H_p(e^{j\omega})|^2 d\omega \tag{29}$$

$$E_\infty = \max_{\omega \in [\omega_s, \pi]} |H_p(e^{j\omega})|, \tag{30}$$

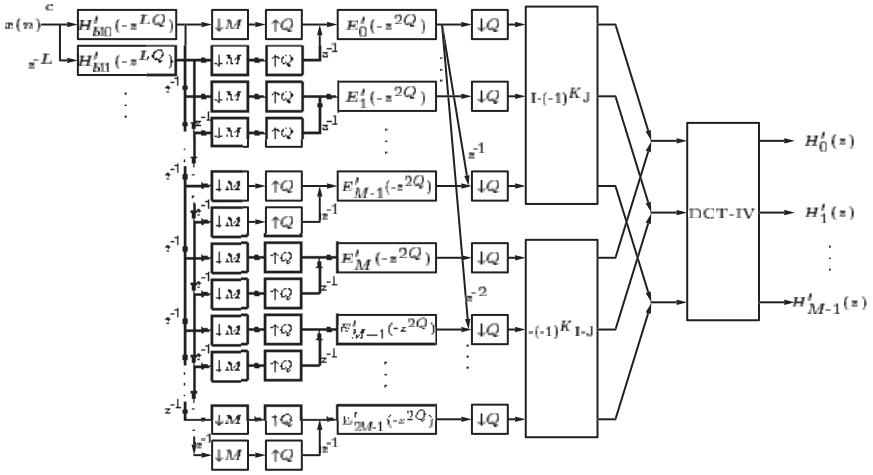

Figure 5. CMFB structure using the FRM approach for the general case with $L = 2K_aM + \frac{M}{K_b}$.

which correspond to the total energy and the maximum magnitude value in the filter's stopband, respectively, where ω_s is the stopband edge frequency. In practice, to control the aliasing distortion and the overall direct transfer of the filter bank, the following constraints are introduced:

$$1 - \delta_1 \leq |T_0(e^{j\omega})| \leq 1 + \delta_1 \tag{31}$$

$$|T_i(e^{j\omega})| \leq \delta_2 \tag{32}$$

for $i = 1, 2, \ldots, (M-1)$ and $\omega \in [0, \pi]$.

In the FRM-CMFB structure, the prototype filter $H_p(z)$ is as given in equation (19), and the approximation problem resides on finding a base filter, a positive masking filter (upper branch), and a negative masking filter (lower branch) that optimize E_2 or E_∞ subject to the constraints given by equations (31) and (32). In this work, for the optimization we used a quasi-Newton algorithm with line search implemented with the command `fmincon` in MATLAB [8]. The gradient vector was determined analytically to reduce the computational burden during the optimization procedure. The functions $T_0(z)$ and $T_i(z)$ for $i = 1, 2, \ldots, (M-1)$ required to impose the desired constraints have an extremely high computational complexity. Some modifications, however, can significantly simplify the problem of evaluating these constraints, as described below.

In the z-domain, equations (3) and (4) become [10]

$$H_m(z) = \alpha_m \beta_m H_p(ze^{\frac{-j(2m+1)\pi}{2M}}) + \alpha_m^* \beta_m^* H_p(ze^{\frac{j(2m+1)\pi}{2M}}) \tag{33}$$

$$F_m(z) = \alpha_m^* \beta_m H_p(ze^{\frac{-j(2m+1)\pi}{2M}}) + \alpha_m \beta_m^* H_p(ze^{\frac{j(2m+1)\pi}{2M}}) \tag{34}$$

for $m = 0, 1, \ldots, (M-1)$, where

$$\alpha_m = e^{\frac{j(-1)^m \pi}{4}}; \quad \beta_m = e^{\frac{-jN_p(2m+1)\pi}{4M}}, \tag{35}$$

where N_p is the prototype filter order. Using these relations in equation (11), we get

$$T_0(z) = \sum_{m=0}^{M-1} \left({\beta_m}^2 H_p^2(ze^{\frac{-j(2m+1)\pi}{2M}}) + {\beta_m^*}^2 H_p^2(ze^{\frac{j(2m+1)\pi}{2M}}) \right) \tag{36}$$

because $({\alpha_m}^2 + {\alpha_m^*}^2) = 0$ and $\alpha_m \alpha_m^* = 1$ for all m.

Using $H_p(z)$ as defined in equation (2), we obtain

$$\begin{aligned}
T_0(z) &= \sum_{m=0}^{M-1} {\beta_m}^2 \left(\sum_{n=0}^{N_p} h_p(n) z^{-n} e^{\frac{j(2m+1)\pi n}{2M}} \right)^2 \\
&\quad + \sum_{m=0}^{M-1} {\beta_m^*}^2 \left(\sum_{n=0}^{N_p} h_p(n) z^{-n} e^{\frac{-j(2m+1)\pi n}{2M}} \right)^2 \\
&= \sum_{m=0}^{M-1} {\beta_m}^2 \left(\sum_{n=0}^{2N_p} a(n) z^{-n} e^{\frac{j(2m+1)\pi n}{2M}} \right) \\
&\quad + \sum_{m=0}^{M-1} {\beta_m^*}^2 \left(\sum_{n=0}^{2N_p} a(n) z^{-n} e^{\frac{-j(2m+1)\pi n}{2M}} \right) \\
&= \sum_{n=0}^{2N_p} a(n) z^{-n} \left[\sum_{m=0}^{M-1} \left({\beta_m}^2 e^{\frac{j(2m+1)\pi n}{2M}} + {\beta_m^*}^2 e^{\frac{-j(2m+1)\pi n}{2M}} \right) \right] \\
&= \sum_{n=0}^{2N_p} a(n) z^{-n} \gamma(n),
\end{aligned} \tag{37}$$

where the coefficients $a(n)$ result from the convolution of $h_p(n)$ with itself, that is,

$$Z\{h_p(n) * h_p(n)\} = \sum_{n=0}^{2N_p} a(n) z^{-n}, \tag{38}$$

and $\gamma(n)$ is defined as

$$\gamma(n) = \begin{cases} 2M(-1)^c, & \text{for } (N_p - n) = 2Mc,\ c \text{ integer} \\ 0, & \text{otherwise.} \end{cases} \tag{39}$$

See the Appendix for a detailed derivation of this expression of $\gamma(n)$.

Similarly, all functions $T_i(z)$ can be evaluated using this simplification, by modulating one of the terms of the convolution in equation (38), as follows:

$$T_i(z) = Z\left\{ \left(e^{\frac{j2\pi in}{M}} h_p(n) * h_p(n) \right) \gamma(n) \right\} \tag{40}$$

Table 1. Figures of merit for the optimized direct-form and FRM prototype filters in Example 1

Figures of merit	Direct form [1]	FRM
Number of coefficients	48	22
δ_1	0.001	0.00087
δ_2 (dB)	−83.6	−88.2
A_r (dB)	−74.0	−77.4
ISI (dB)	−62.0	−63.1
ICI (dB)	−80.4	−82.0

for $i = 1, 2, \ldots, (M-1)$. Due to the symmetry in the modulation function, $T_i(z) = T_{M-i}(z)$. Hence, one may evaluate functions $T_i(z)$ only for $i = 1, 2, \ldots, \lfloor M/2 \rfloor$, where the operator $\lfloor x \rfloor$ denotes the integer part of x.

6. Design examples

A quasi-Newton algorithm with line search was applied to both direct-form (standard equiripple filter) and FRM realizations of the CMFB prototype filter aiming to achieve improved performances with respect to E_∞ given in equation (30). The prototype filters were used on a TMUX system, and the parameters of interest of this structure, namely, the passband ripple, δ_1, aliasing interference, δ_2, minimum stopband attenuation, A_r, ISI, and ICI, were measured in each case.

Example 1. This example compares the realization of a CMFB with $M = 8$ bands and $\rho = 1$, based on both direct and FRM implementations. The overall order of the prototype filters in both cases was set to $N_p = 2KM - 1 = 95$, resulting in a factor of $K = 6$ for the polyphase decomposition. The direct-form realization was optimized in [1], and its final characteristics are included in Table 1. The FRM structure was developed with an interpolation factor $L = 4$, thus allowing one to discard the lower branch of the FRM diagram. The orders of the base and positive masking filters were $N_b = 18$ and $N_m = 23$, respectively, yielding an overall order of $N_p = LN_b + N_m = 95$ for the FRM filter. In this case, however, we have solely 22 distinct coefficients, considering their symmetry in the base and masking filter transfer functions.

Table 1 summarizes the results achieved by the optimization of the FRM prototype filter for the CMFB. As can be verified from this table, the FRM-CMFB presents a superior performance compared to the optimized direct-form design. Clearly, the large number of direct-form parameters being optimized prevented the optimization procedure in [1] from reaching its global solution. The magnitude responses of both the optimized FRM prototype filter and the complete FRM-CMFB are shown in Figures 6 and 7, respectively. Figure 8 illustrates the direct-path $T_0(e^{j\omega})$ function.

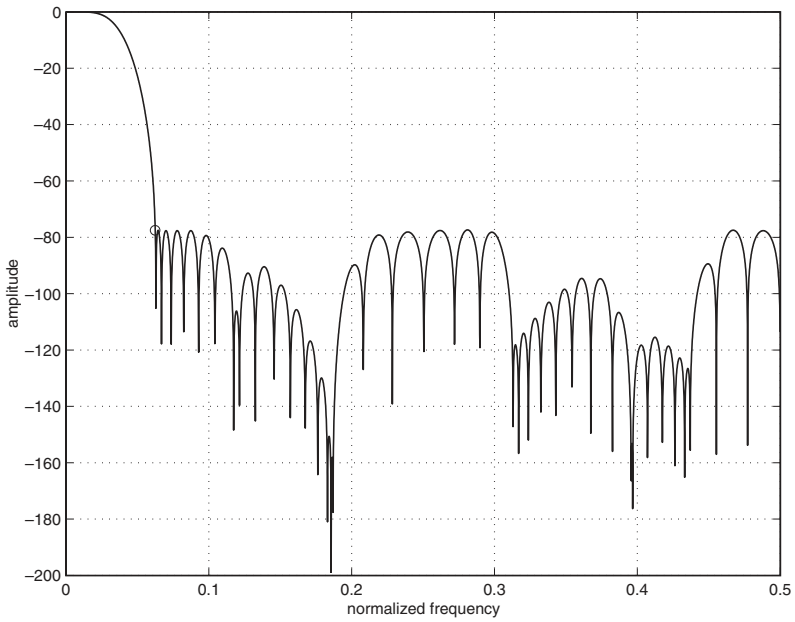

Figure 6. Magnitude response of optimized FRM prototype filter in Example 1.

Example 2. This example compares the realization of a CMFB with $M = 32$ bands and $\rho = 1$, based on both direct-form and FRM implementations. The direct-form prototype filter was optimized in [9], which used an order $N_p = 2KM - 1 = 511$, where $K = 8$ was chosen to obtain good stopband attenuation. The FRM structure was developed with an interpolation factor $L = 4$. The orders of the base and positive masking filters were $N_b = 111$ and $N_m = 67$, respectively, also yielding an overall order of $N_p = LN_p + N_m = 511$, with, however, only 90 distinct coefficients.

Table 2 presents the results obtained in [9] for the optimized direct-form filter and the ones obtained with the optimized FRM-CMFB prototype filter. Although both realizations achieved similar performances, the FRM-CMFB design has been shown to be simpler to optimize because of its reduced number of coefficients when compared to the direct-form design. In fact, the performance of the FRM-CMFB could be improved by increasing the orders of the base or masking filters, while still keeping its computational complexity much lower than the one for the direct-form filter.

Figures 9 and 10 show the magnitude responses of the optimized FRM prototype filter and the complete FRM-CMFB, respectively.

Example 3. The third example is based on a filter bank with $M = 1024$ and $\rho = 0.1$. The desired stopband attenuation is $A_r = -60$ dB. These characteristics

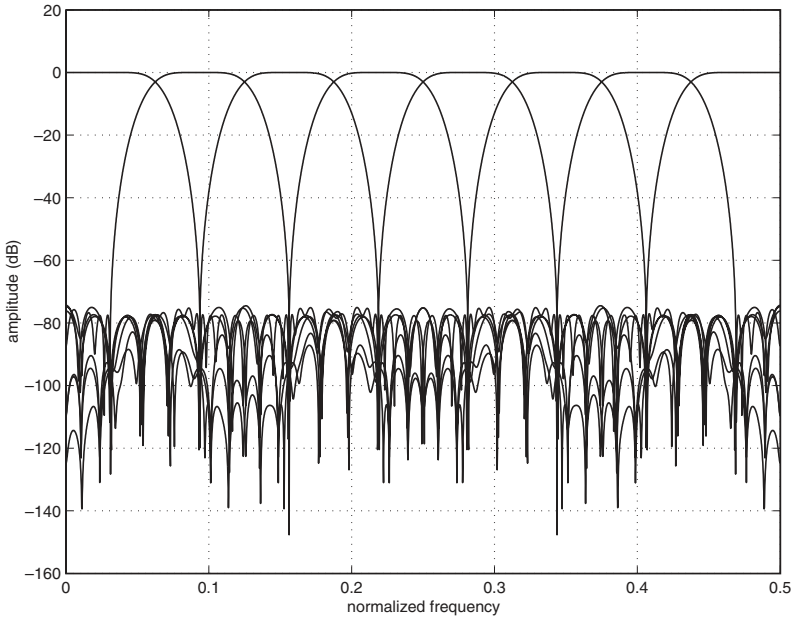

Figure 7. Magnitude response of optimized FRM-CMFB in Example 1.

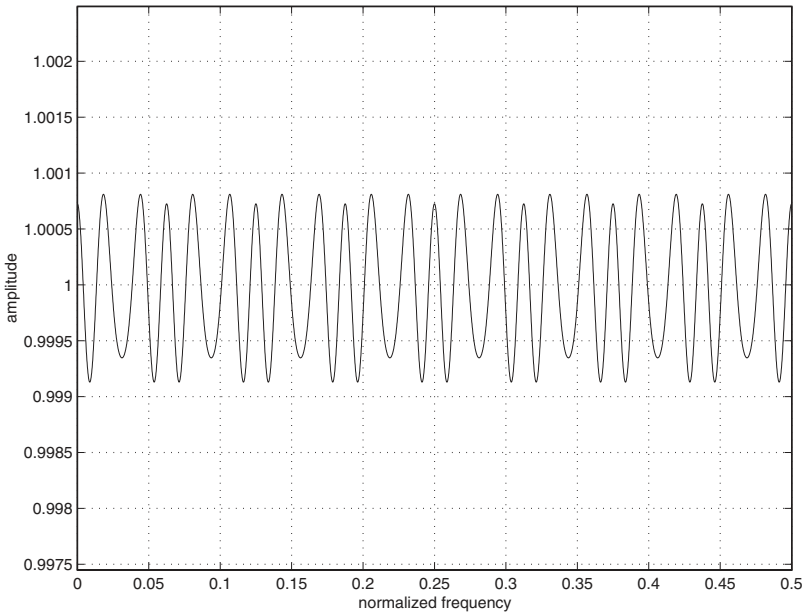

Figure 8. Function $T_0(z)$ for optimized FRM-CMFB in Example 1.

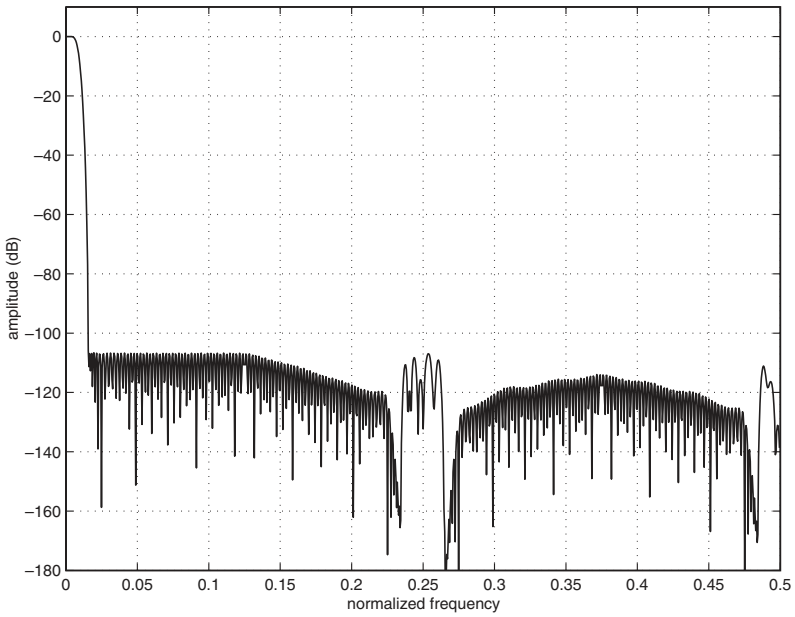

Figure 9. Magnitude response of optimized FRM prototype filter in Example 2.

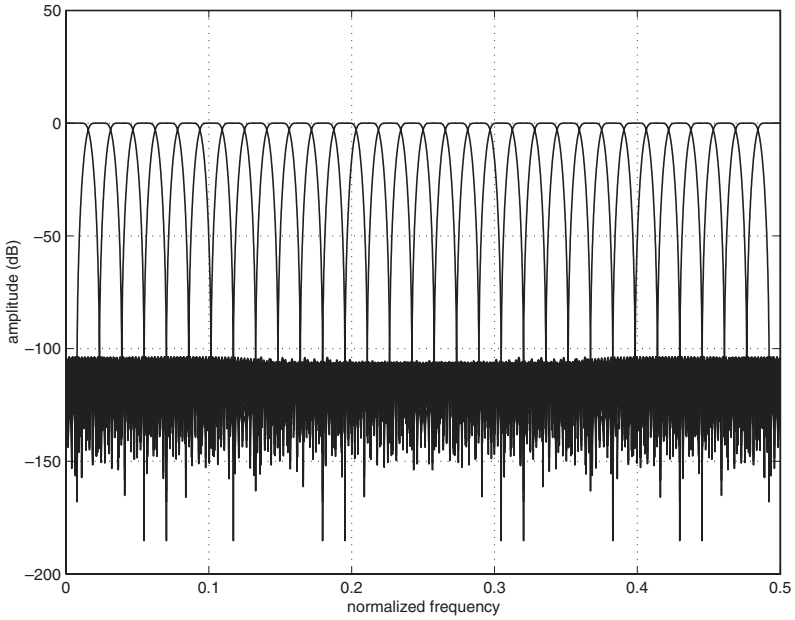

Figure 10. Magnitude response of optimized FRM-CMFB in Example 2.

Table 2. Figures of merit for the optimized direct-form and FRM prototype filters in Example 2

Figures of merit	Direct form [9]	FRM
Number of coefficients	256	90
δ_1	0.0001	0.0001
δ_2 (dB)	−99.0	−98.5
A_r (dB)	−106.0	−105.9
ISI (dB)	−83.4	−81.7
ICI (dB)	−86.9	−94.9

Table 3. Figures of merit for the standard and optimized FRM prototype filters in Example 3

Figures of merit	Standard FRM	Optimized FRM
Number of coefficients	945	945
δ_1	0.004	0.004
δ_2 (dB)	−60.6	−64.4
A_r (dB)	−63.8	−67.6
ISI (dB)	−123.2	−126.4
ICI (dB)	−121.2	−124.9

lead to a prototype filter that is unfeasible to design using the direct-form realization with standard approximation routines. So, in this example, we compare the optimized FRM-CMFB with its nonoptimized version. In both cases, the FRM prototype filter was characterized by $N_b = 234$, $L = 384$, and $N_m = 1653$, yielding an overall filter order $N_p = 91,509$ and a total of $N = 945$ distinct coefficients to be optimized. Table 3 shows the results of this optimization process.

Figure 11 shows the optimized prototype filter in a reduced grid of frequencies (a tenth of the original) for better visualization, whereas Figure 12 depicts 32 out of the 1024 bands of the optimized FRM-CMFB in this example.

7. Conclusions

A new design procedure for optimizing the prototype filter of a CMFB was presented. The new method is based on the use of a prototype filter designed with the FRM approach, thus constituting the FRM-CMFB structure. A quasi-Newton method with line search is used to perform minimization of the maximum value of the magnitude response within the filter's stopband. Other objective functions, such as the filter's total stopband energy, may be considered in a similar fashion. Constraints related to ISIs and ICIs are considered, in an extremely simplified manner, in a TMUX configuration. The result is a numerically robust optimization

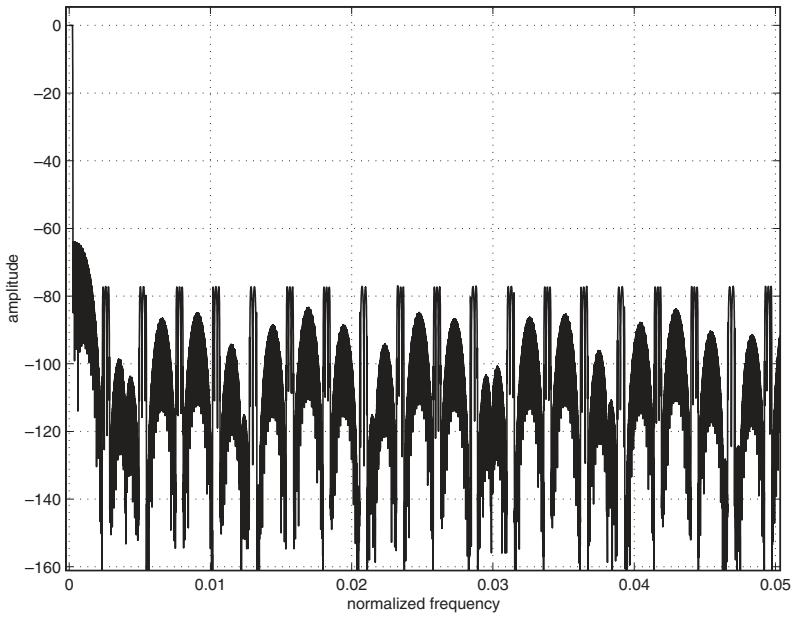

Figure 11. Magnitude response of optimized FRM prototype filter in Example 3.

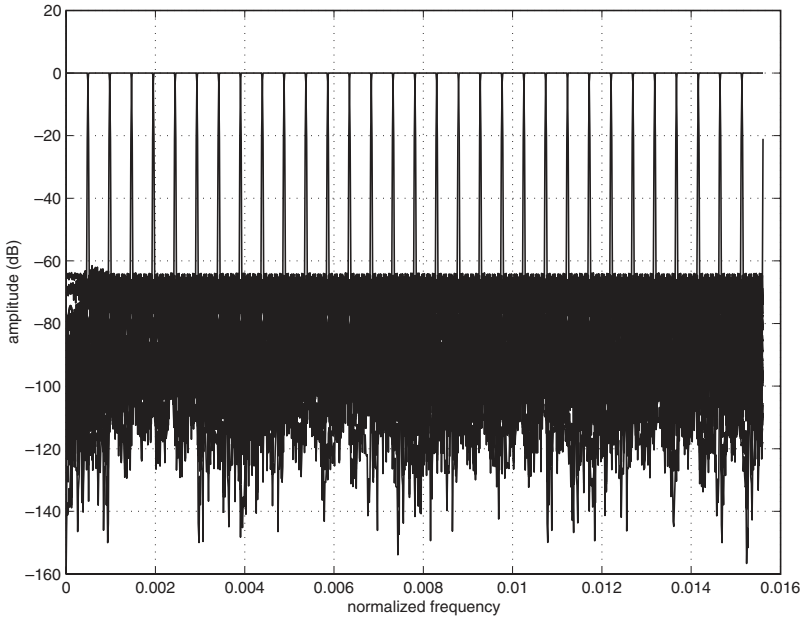

Figure 12. Partial magnitude response (32 bands out of 1024) of optimized FRM-CMFB in Example 3.

procedure that yields very efficient filter banks with respect to several figures of merit, including the number of coefficients capitalized by the FRM-CMFB structure. In addition, the reduced number of multipliers of the FRM-CMFB structure allows the design of very high-order filter banks with high selectivity, a feature not available so far.

Appendix

From equation (37), using the definition of β_m given by equation (35), we get

$$\gamma(n) = \sum_{m=0}^{M-1} e^{\frac{-j(N_p-n)(2m+1)\pi}{2M}} + \sum_{m=0}^{M-1} e^{\frac{j(N_p-n)(2m+1)\pi}{2M}}. \tag{41}$$

If $(N_p - n)$ is not a multiple of $2M$, then

$$\begin{aligned}
\gamma(n) &= e^{\frac{-j(N_p-n)\pi}{2M}} \left[\frac{1 - e^{-j(N_p-n)\pi}}{1 - e^{\frac{-j(N_p-n)\pi}{M}}} \right] + e^{\frac{j(N_p-n)\pi}{2M}} \left[\frac{1 - e^{j(N_p-n)\pi}}{1 - e^{\frac{j(N_p-n)\pi}{M}}} \right] \\
&= e^{\frac{-j(N_p-n)\pi}{2}} \frac{\sin\left[\frac{(N_p-n)\pi}{2}\right]}{\sin\left[\frac{(N_p-n)\pi}{2M}\right]} + e^{\frac{j(N_p-n)\pi}{2}} \frac{\sin\left[\frac{(N_p-n)\pi}{2}\right]}{\sin\left[\frac{(N_p-n)\pi}{2M}\right]} \\
&= \frac{2\cos\left[\frac{(N_p-n)\pi}{2}\right] \sin\left[\frac{(N_p-n)\pi}{2}\right]}{\sin\left[\frac{(N_p-n)\pi}{2M}\right]} \\
&= \frac{\sin\left[(N_p-n)\pi\right]}{\sin\left[\frac{(N_p-n)\pi}{2M}\right]},
\end{aligned} \tag{42}$$

which is null for all n.

If, however, $(N_p - n) = 2Mc$, with c integer, equation (41) becomes

$$\gamma(n) = \sum_{m=0}^{M-1} 2\cos\left[c(2m+1)\pi\right] = \sum_{m=0}^{M-1} 2(-1)^c, \tag{43}$$

yielding the expression in equation (39).

References

[1] J. Alhava and A. Viholainen, Implementation of nearly perfect reconstruction cosine-modulated filter banks, *Proc. FinSig*, 222–226, Oulu, Finland, 1999.

[2] L. C. R. de Barcellos, S. L. Netto, and P. S. R. Diniz, Design of FIR filters combining the frequency-response masking and the WLS-Chebyshev approaches, *Proc. IEEE Int. Symp. Circuits and Systems*, II, 613–616, Sydney, Australia, May 2001.

[3] P. S. R. Diniz, L. C. R. de Barcellos, and S. L. Netto, Design of cosine-modulated filter bank prototype filters using the frequency-response masking approach, *Proc. IEEE Int. Conf. Acoustics, Speech, and Signal Processing*, VI, P4.6 1–4, Salt Lake City, UT, May 2001.

[4] P. S. R. Diniz and S. L. Netto, On WLS-Chebyshev FIR digital filters, *J. Circuits Systems Comput.*, 9, 155–168, 1999.
[5] N. J. Fliege, *Multirate Digital Signal Processing*. Chichester, NY: John Wiley & Sons, 1994.
[6] Y. C. Lim, Frequency-response masking approach for the synthesis of sharp linear phase digital filters, *IEEE Trans. Circuits and Systems*, CAS-33, 357–364, Apr. 1986.
[7] Y. C. Lim and Y. Lian, The optimal design of one- and two-dimensional FIR filters using the frequency response masking technique, *IEEE. Trans. Circuits and Systems II*, 40, 88–95, Feb. 1993.
[8] *MATLAB Optimization Toolbox: User's Guide*, The MathWorks Inc., Natick, MA, 1997.
[9] T. Saramäki, A generalized class of cosine-modulated filter banks, *Proc. TICSP Workshop on Transforms and Filter Banks*, 336–365, Tampere, Finland, June 1998.
[10] P. P. Vaidyanathan, *Multirate Systems and Filter Banks*, Englewood Cliffs, NJ: Prentice-Hall, 1993.
[11] A. Viholainen, T. Saramäki, and M. Renfors, Cosine-modulated filter bank design for VDSL modems, *Proc. IEEE Int. Workshop Intelligent Signal Processing and Communic. Systems*, 143–147, Melbourne, Australia, Nov. 1998.
[12] A. Viholainen, T. Saramäki, and M. Renfors, Nearly perfect reconstruction cosine-modulated filter bank design for VDSL modems, *Proc. IEEE Int. Conf. Electronics, Circuits, and Systems*, 373–376, Paphos, Greece, Sept. 1999.